SAND2017-1512C

A multifidelity multilevel Monte Carlo method for uncertainty propagation in aerospace applications

Geraci Gianluca*

Flow Physics and Computational Engineering, Stanford University, Stanford, CA 94305, USA

Michael S. Eldred†

Computer Science Research Institute, Sandia National Laboratories, Albuquerque, NM, 87185, USA

Gianluca Iaccarino‡

Flow Physics and Computational Engineering, Stanford University, Stanford, CA 94305, USA

The accurate evaluation of the performance of complex engineering devices needs to rely on high-fidelity numerical simulations and the systematic characterization and propagation of uncertainties. Several sources of uncertainty may impact the performance of an engineering device through operative conditions, manufacturing tolerances, and even physical models. In the presence of multiphysics systems the number of the uncertain parameters can be fairly large and their propagation through the numerical codes still remains prohibitive because the overall computational budget often allows for only an handful of such high-fidelity realizations. On the other side, common engineering practice can take advantage from a solid history of development and assessment of so called low-fidelity models which albeit less accurate are often capable to at least capture overall trends and parameter dependencies of the system. In this contribution we address the forward propagation of uncertainty parameters relying on statistical estimators built on sequences of numerical and physical discretizations which are provably convergent to the high-fidelity statistics, while exploiting low-fidelity computational models to increase the reliability and confidence in the numerical predictions. The performances of the approaches are presented by means of two fairly complicated aerospace problems, namely the aero-thermo-structural analysis of a turbofan engine nozzle and a flow through a scramjet-like device.

Nomenclature

$\mathbf{x}$	Spatial coordinates
$\boldsymbol{\xi}$	Vector of stochastic parameters
$p(\boldsymbol{\xi})$	Joint probability density function of $\boldsymbol{\xi}$
t	Temporal coordinate
d	Number of stochastic parameters
Ω	Physical space
Ξ	Stochastic space
T	Temporal space
Q	Generic Quantity of Interest
M	Number of discretization degrees-of-freedom
N	Number of stochastic realizations
ℓ	ML dicretization level

*PostDoctoral Research Fellow. Now PostDoctoral Appointee, Optimization and Uncertainty Quantification Department, Sandia National Laboratories, AIAA Member

†Distinguished Member of the technical staff, Optimization and Uncertainty Quantification Department, AIAA Associate Fellow

‡Associate Professor, Mechanical Engineering Department, AIAA Associate Fellow

$\mathbb{E}[Q]$ Expected value of Q
$\mathbb{V}ar(Q)$ Variance of Q
ρ Pearson's correlation coefficient between low- and -high-fidelity models

$\hat{\mathbb{E}}[Q]$ Estimated expected value for Q
$\hat{Q}^{MC}_{M,N}$ Monte Carlo estimator for $\mathbb{E}[Q_M]$ based on N samples
$\hat{Q}^{\mathrm{HF,CV}}_{M,N}$ multifidelity control variates MC estimator for Q^{HF}_M
Λ Multifidelity variance reduction
λ Lagrange multiplier
$\mathcal{C}$ Computational cost
τ_ℓ Ratio between variances of $\mathring{Y}^{\mathrm{LF}}_\ell$ and Y^{LF}_ℓ
θ_ℓ Ratio between covariances (HF,LF) for $\mathring{Y}^{\mathrm{LF}}_\ell$ and Y^{LF}_ℓ
w Cost ratio between HF and LF

Superscripts

(i) ith sample
HF High-fidelity
LF Low-fidelity

I. Introduction

Numerical predictions of the performance of complex multi-physics engineering devices cannot leave aside the evaluation of the uncertainies' impact. In presence of complex high-fidelity multi-physics numerical codes the computational budget is often limited to an handful of realizations whereas the number of uncertain parameters can be fairly large. In aerospace and aerodynamics applications is also very common to deal with systems or devices which exhibit high non linearity and even discontinuous responses, as for instance in the case of presence of shock waves or large structural displacements and deformations. Therefore, the combination of high dimensional parameter spaces (referred in literature as *curse of dimensionality*[3]), non-linear responses and high computational cost of a single deterministic realization still constitutes a barrier for uncertainty quantification (UQ). Indeed common UQ techniques, as for instance Stochastic Collocation or Polynomial Chaos,[22] are very efficient in the presence of parameter spaces of moderate dimension and smooth responses. In recent years, to overcome these difficulties many improvements have been proposed,[7,31] however in high-dimensional spaces their applicability still remains limited. More recently, statistical sampling methods, which historically were among the first ones to be proposed, have re-gained popularity. The seminal Monte Carlo (MC) method has been generalized to multilevel approaches leading to the so-called Multilevel MC method (MLMC). The MLMC method was first introduced in the context of numerical quadrature[19] and subsequently generalized by Giles to enhance the MC path simulation for stochastic differential equations in finance.[18] More recently, MLMC has been applied to a variety of problems ranging from elliptic, parabolic and hyperbolic problems.[5,2,24] The MLMC method has been demonstrated to be superior to MC in all possible scenarios, and it is a good candidate for many applications which actually are intractable by other UQ methods. Despite all these advantages, the number of simulations required remains very high, even if it stays more favorable compared to other techniques. At the same time, in the engineering practice a solid history of use and assessment of low-fidelity models is present. For instance, in aerodynamics a sequences of models and numerical methods have been developed in the last fifty years to assist the engineers in the preliminary design stages. Nowadays the increased computational capabilities led to a broader use of high-fidelity simulations even in the preliminary stages of design. However, the need for UQ can still motivate the use of low-fidelity computational models which albeit less accurate are often capable to capture general trend and parameters dependencies of the model. The goal of this work is to show how the combination of multilevel techniques and low-fidelity models, by means of the so-called control variates approach, can allow to generate more reliable statistics in the context of forward UQ studies for large multi-physics applications for which the computational budget would make the use of other UQ methods very challenging. To demonstrate the flexibility of the algorithm and the advantages of its application with respect to other sampling strategies two applications are presented. The first is an aero-thermo-structural analysis of the nozzle of a F100-PW-220 turbofan engine which powers the Northrop Grumman's unmanned combat vehicle X-47B.[12] For this problem a set of operative and manufacturing uncertainties is considered. A multi-physics analysis is performed for the flow inside the nozzle and the thermal and mechanical loading on the surrounding struc-

ture. The second example is a unit model inspired by the HIFiRE (Hypersonic International Flight Research and Experimentation) Supersonic Combustion RAMJET (SCRAMJET) engine configuration designed at NASA Langley Research Center.[6,21] The unit problem used in this manuscript targets the subdomain of the primary injector section of this SCRAMJET and focuses on the interaction betweeen the fuel jet and the supersonic air crossflow without combustion. The remainder of the manuscript is organized as follows. In Sec. II we furnish some context regarding the meaning of multilevel and multilevel hierarchies in engineering applications. Sampling methods, which are the fundamental tool we use in all the following derivations, are introduced in Sec. III. Afterward, we describe how to build multifidelity estimators, Sec. IV, multilevel estimators, Sec. V, and eventually how to combine the two ideas to obtain multilevel-multifidelity estimators in Sec. VI. A brief discussion of some relevant issues impacting on the practical implementation of the algorithms is reported in Sec. VII. We focus on the deployment of the MLMF algorithm on two aerospace engineering problems, namely an aero-thermo-structural analysis of a nozzle and a unit problem inspired by the supersonic combustion SCRAMJET engine HIFiRE. These two applications are briefly described in Sections VIII.A and VIII.B, respectively. Eventually, the numerical results obtained for the UQ forward analysis of the two problems mentioned above are reported in Sec. IX. Conclusions and perspectives are drawn in Sec. X.

II. Multilevel/Multifidelity context in engineering applications

In this work we are interested in two complex multi-physics aerospace problems for which the computational cost limits the number of total runs available making the applicability of classical UQ forward algorithms very challenging. In general, the overall analysis of complex engineering devices consists in at least three fundamental stages: physical modeling, numerical discretization, and Verification and Validation (V&V) which encompasses a forward UQ phase. These three steps should not be intended as part of a complete sequential process, but instead are steps to be taken in the context of an iterative process aiming to verify the validity of the hypotheses and approximations made at each stage. The first stage, referred here as physical modeling, is the process of selecting the adequate level of physical description which suits the application, i.e. equation or system of equations which govern the system. For instance, examples of different physical choices in Computational Fluid Dynamics (CFD) are laminar versus turbulent flows, viscous versus inviscid fluid, ideal versus real gas thermodynamics equation of state *etc.* The discretization step is associated to the choice of the numerical algorithms and parameters which allows the accurate resolution of the selected set of physical equations. It should be evident that this step is not completely decoupled from the previous stage since different algorithms are suited for different physical models. For instance, in the context of CFD, different physical hypotheses may lead to complete different mathematical properties of the equations, as for instance compressible versus incompressible hypothesis for a fluid lead to a system of equations which are hyperbolic or elliptic in nature which in turn might require completely different numerical algorithms, for instance explicit versus implicit time stepping procedures. The discretization step comes also with associated parameters which impact on the accuracy of the numerical modeling. For instance, the most common parameters in the numerical resolution of partial differential equations (PDEs) are the spatial and time discretization steps. The role of the V&V step is to rigorously assess that the combination of physical and numerical discretization are adequate choices for the problem and also to equip the numerical predictions with confidence intervals. Indeed, confidence intervals naturally arise from the propagation of uncertainties that come from the first two stages. In this manuscript we are interested in the forward propagation step contained in V&V which we refer here generically as forward Uncertainty Quantification (UQ) that consists in the numerical propagation of all the sources of uncertainties through the numerical code in order to provide confidence intervals for the desired Quantities of Interest (QoIs). Often a very challenging task of V&V is to provide a framework to rigorously balance the errors that come from the discretization step and from stochastic variability. This aspect constitutes another element of coupling between the physical and discretization modeling. Generally it is needed to adjust the numerical discretization to match the accuracy provided by the chosen physical model avoiding to under- or over-resolve the governing equations. Physical and discretization models are based on distinct principles, but they also share some important features that are instrumental to our work. In particular, it is always possible to identify a direction of increasing accuracy defined in an abstract way as a direction of diminishing 'distance' with respect to a true solution which at the same time coincides with an increasing computational cost. In the following, we refer to this direction as hierarchy of models or discretization levels. For instance, in CFD a clear example of hierarchy between

physical models might be potential flow, Euler equations, Navier-Stokes equations. However, we stress here that the choice of an adequate physical model depends on the application and the relevant quantity of interest even if in principle an higher accurate model is present in the hierarchy. For instance, computing the coefficient of lift for an airfoil flying at low angle of attach in transonic condition might require to solve Euler equation to satisfy the accuracy needed in practical calculations even if in principle the full accurate resolution of the flow field would require to solve the Navier-Stokes equations. In some cases one could consider the possibility of the existence of peers of models/discretizations for which the behavior of the pair computational cost/accuracy is not known *a priori* for a fixed problem. For instance, in the context of Reynolds Averaged Navier-Stokes equations (RANS) for a complex flow the accuracy of k-ϵ versus k-ω models can be difficult to know beforehand. In the context of the present work we exclude the previous case and we focus on well defined hierarchies (*i.e.* increasing computational cost for increasing accuracy) of models and numerical discretizations (in the following we will refer to it only as discretization). In particular, we limit ourselves to a scenario in which several discretization levels are available (multilevel), but only two physical models (multifidelity) are available. We refer to them as low- and high-fidelity. Moreover, we assume that the applications of interest strictly require the use of the high-fidelity computation to capture features of the solution which are needed for the accurate evaluation of the QoIs, and that the cost of the high-fidelity model is such that requires large-scale computational resources to provide only few realizations. For the UQ context we consider the following scenario, justified by the aerospace applications selected in this work: high-dimensional stochastic spaces, *i.e* large number of uncertainty parameters to propagate through the numerical code and lack of estimation on the accuracy for the QoIs which prevents, at least in the preliminary stages of the analysis, to take advantage to the fast convergence of methods like PC. In the presence of less extreme hypothesis, alternative multifidelity approaches based on PC and stochastic collocation reconstructions have already been demonstrated to be effective.[26,8] According to the UQ context defined above a natural candidate for the UQ propagation is the Monte Carlo (MC) method which does not requires any degree of regularity of the solution to converge and retains its order of convergence independently from the number of stochastic dimensions. Also, in the context of multiphysics applications MC offers another key advantage which is its non-intrusive character. More specifically, non-intrusive propagation techniques are such that the deterministic code can be used as a black box avoiding to develop *ad hoc* codes and solvers. As a result, its flexibility decreases the time needed for the deployment of the algorithm on a new application. In the context of our research, both the robustness and the non-intrusiveness of MC are features that we want to preserve in developing more efficient UQ algorithms.

III. Sampling methods

Monte Carlo algorithm, historically the first developed for stochastic simulations, is popular due to its simplicity, flexibility and provably convergent behavior. Let consider here an abstract PDE governing the evolution of a QoI, $Q = Q(\mathbf{x}, \boldsymbol{\xi}, t)$, where $\mathbf{x} \in \Omega \subset \mathbb{R}^n$ and $t \in T \subset \mathbb{R}^+$ are the spatial and temporal coordinates respectively and $\boldsymbol{\xi} \in \Xi \subset \mathbb{R}^d$ denotes a vector of d random variables. The role of the random parameters is to represent the effect of sources of uncertainties in the system, as for instance might happen for the operative conditions of a flight device or the manufacture tolerances of its components. We are interested in the evaluations of statistics of Q, for instance its expected value $\mathbb{E}[Q]$, over the space Ξ when a discretization of the PDE is assumed. The definition of the problem also requires the specification of the probability density distribution (pdf) for each of the random parameters in order to compute statistics. We do not assume here any particular shape for the joint probability distribution $p(\boldsymbol{\xi})$ of the random parameters $\boldsymbol{\xi}$ which in general might be even correlated.

For simplicity of exposure the case in which the discretization level is directly related to the number of degrees-of-freedom M in the spatial and time spaces tessellation is considered here. We assume that $Q_M \to Q$ for $M \to \infty$, therefore $\mathbb{E}[Q_M] \to \mathbb{E}[Q]$ for $M \to \infty$. Accuracy and practical requirements are supposed to guide the selection of the resolution M to be employed for the numerical resolution of the PDEs and the subsequent evaluation of Q. A MC estimator for the expected value of Q_M, based on N realizations, is defined as

$$\mathbb{E}[Q_M] = \int_\Xi Q(x, t, \boldsymbol{\xi}) p(\boldsymbol{\xi}) \mathrm{d}\boldsymbol{\xi} \simeq \hat{Q}^{MC}_{M,N} = \frac{1}{N} \sum_{i=1}^{N} Q^{(i)}_M, \tag{1}$$

where we denote a single ith realization $Q^{(i)}_M = Q(\mathbf{x}, t, \boldsymbol{\xi}^{(i)})$ evaluated for $\boldsymbol{\xi}^{(i)}$ which is drawn according to

the distribution $p(\boldsymbol{\xi})$. Important features of the MC estimator can be derived from the analysis of the mean square error (MSE)

$$\mathbb{E}\left[(\hat{Q}_{M,N}^{MC} - \mathbb{E}\left[Q\right])^2\right] = N^{-1}\mathbb{V}ar\left(Q_M\right) + \left(\mathbb{E}\left[Q_M - Q\right]\right)^2. \tag{2}$$

Of great importance for our analysis is to identify the two main contributions to MSE, namely the variance of the estimator $N^{-1}\mathbb{V}ar\left(Q_M\right)$ and the deterministic bias $\left(\mathbb{E}\left[Q_M - Q\right]\right)^2$. In order to obtain accurate solutions the deterministic bias must be reduced by using high-fidelity models at sufficiently large resolution, *i.e.* a large value of M in our notation. Therefore in the context of UQ the use of high-fidelity simulations is at some level unavoidable. However, MC estimators are inherently stochastic in nature, *i.e.* each set of realizations $\{\boldsymbol{\xi}\}_{i=1}^{N}$ would produce a different result, therefore the estimator itself $\hat{Q}_{M,N}^{MC}$ own a variance associated to it. It is possible to show that the distribution of the values of $\hat{Q}_{M,N}^{MC}$ is a standard normal variable, therefore the quantification of its variance directly enables to equip the statistical estimation with a confidence interval. Indeed, for the UQ prediction not only the single deterministic realization must be accurate (high resolution and high-fidelity), but also the statistics needs to be computed on a large set of N realizations in order to reduce the variability of the results. A closed inspection of the variance term in Eq. (2) reveals that it is directly proportional to the variance of the QoI and inversely proportional to the number of realizations N. Therefore, in MC simulation is common to increase the number of realizations N in order to reduce the stochastic contribution to the MSE up to obtain a balance with the deterministic bias. The remainder of this contribution is focused on alternative strategies to efficiently reduce the variance term $N^{-1}\mathbb{V}ar\left(Q_M\right)$ resorting to less accurate (low-fidelity and/or low resolution) approximations of Q_M which being less computationally expensive enable us to generate a larger set of their realizations. Eventually low variance estimators lead to smaller confidence intervals for the estimated statistics, hence greater a confidence in their results can be placed.

IV. Multifidelity estimators

In order to reduce the variance term $N^{-1}\mathbb{V}ar\left(Q_M\right)$ in Eq. (2) beside the direct approach of increasing N, many more sophisticated alternatives have been proposed.[23,29,27] An incomplete list might include stratified sampling, importance sampling, Latin hypercube lattice, deterministic Sobol' sequences and control variates method. We focus in this work on the control variates (CV) method and in particular we present in this section how to use it where low- and high-fidelity models are available. In the following to distinguish between fidelity levels we use the superscript LF for low and HF for high-fidelity, respectively.

It is always possible to re-write the generic QoI obtained from high-fidelity computations Q_M^{HF} adding a term which depends only on low-fidelity realizations

$$Q_M^{\mathrm{HF,CV}} = Q_M^{\mathrm{HF}} + \alpha\left(Q_M^{\mathrm{LF}} - \mathbb{E}\left[Q_M^{\mathrm{LF}}\right]\right), \tag{3}$$

where Q_M^{LF} is the approximation of Q given by a low-fidelity model for which a fixed discretization level M is chosen. For the sake of completeness it is necessary to specify that in principle the HF and LF model can have distinct discretizations, therefore the number M of DOFs of the discretization must be intended as independent for each model. However, we make use of the same symbol to make evident that we are assuming a pairing of the two models at a resolution M. The expected value of Eq. (3) is equal to $\mathbb{E}\left[Q_M^{\mathrm{HF}}\right]$ independently from the value of α, therefore a MC estimator for $Q_M^{\mathrm{HF,CV}}$ is unbiased, *i.e.* $\hat{Q}_M^{\mathrm{HF,CV}} \to \hat{Q}_M^{\mathrm{HF}}$ for $N \to \infty$

$$\hat{Q}_{M,N}^{\mathrm{HF,CV}} = \hat{Q}_{M,N}^{\mathrm{HF}} + \alpha\left(\hat{Q}_{M,N}^{\mathrm{LF}} - \mathbb{E}\left[Q_M^{\mathrm{LF}}\right]\right) \tag{4}$$

At the same time, we can use the additional degree-of-freedom represented by α to obtain a more efficient estimator; indeed the variance of $\hat{Q}_{M,N}^{\mathrm{HF,CV}}$ is

$$\mathbb{V}ar\left(\hat{Q}_{M,N}^{\mathrm{HF,CV}}\right) = \mathbb{V}ar\left(\hat{Q}_{M,N}^{\mathrm{HF}}\right) + \alpha^2\mathbb{V}ar\left(\hat{Q}_{M,N}^{\mathrm{LF}}\right) + 2\alpha\mathrm{Cov}\left(\hat{Q}_{M.N}^{\mathrm{HF}}, \hat{Q}_{M,N}^{\mathrm{LF}}\right), \tag{5}$$

and it can be minimized requiring $\mathrm{d}\mathbb{V}ar\left(\hat{Q}_{M,N}^{\mathrm{HF},CV}\right)/\mathrm{d}\alpha = 0$ at which corresponds

$$\alpha = -\rho\frac{\mathbb{V}ar^{1/2}\left(\hat{Q}_{M,N}^{\mathrm{HF}}\right)}{\mathbb{V}ar^{1/2}\left(\hat{Q}_{M,N}^{\mathrm{LF}}\right)} = -\rho\frac{\mathbb{V}ar^{1/2}\left(Q_M^{\mathrm{HF}}\right)}{\mathbb{V}ar^{1/2}\left(Q_M^{\mathrm{LF}}\right)}, \tag{6}$$

where the Pearson's correlation coefficient between the estimators for the LF and HF (or equivalently Q_M^{HF} and Q_M^{LF}) is denoted as ρ.

Finally, the minimized variance of the MC control variates estimator is

$$\mathbb{V}ar\left(\hat{Q}_{M,N}^{\mathrm{HF,CV}}\right) = \mathbb{V}ar\left(\hat{Q}_M^{\mathrm{HF}}\right)\left(1-\rho^2\right), \tag{7}$$

which guarantees always a variance reduction with respect to the standard MC estimator since $0 < \rho^2 < 1$.

We have assumed in the analysis above that the expected value $\mathbb{E}\left[Q_M^{\mathrm{LF}}\right]$ is known exactly or at least is available with higher accuracy from previous studies. Although this situation may occur when the low fidelity model is an analytical model, in many engineering applications it might be necessary to consider an online evaluation of this term during the UQ stage.

An efficient way of accomplishing this task has been proposed in literature with the name of estimated control means[29] and used to build multifidelity estimator for optimization under uncertainty[27] and forward UQ.[15] We report here the main results and invite the reader to refer to the above cited literature for additional details. The main hypothesis that we use is to compute $\mathbb{E}\left[Q_M^{\mathrm{LF}}\right]$ by means of a MC estimator with a set of realizations greater than N. In particular, we use a set of N identical realizations to evaluate $\hat{Q}_{M,N}^{\mathrm{HF}}$, $\hat{Q}_{M,N}^{\mathrm{LF}}$, and subsequently we enlarge this set using an additional and independent set of Δ^{LF} realizations. To make evident the distinction between the two sets we use N^{HF} to denote the realizations needed for the HF model and we parametrize Δ^{LF} as proportional to it according to $\Delta^{\mathrm{LF}} = rN^{\mathrm{HF}}$. The MC estimator for $\mathbb{E}\left[Q_M^{\mathrm{LF}}\right]$ can be written as

$$\mathbb{E}\left[Q_M^{\mathrm{LF}}\right] \simeq \hat{\mathbb{E}}\left[Q_M^{\mathrm{LF}}\right] = \frac{1}{(1+r)N^{\mathrm{HF}}} \sum_{i=1}^{(1+r)N^{\mathrm{HF}}} Q_M^{\mathrm{LF},(i)}, \tag{8}$$

which plugged in Eq. (4) lead to the following variance (after the minimization)

$$\mathbb{V}ar\left(\hat{Q}_{M,N}^{\mathrm{HF},CV}\right) = \mathbb{V}ar\left(\hat{Q}_M^{\mathrm{HF}}\right)\left(1-\frac{r}{1+r}\rho^2\right). \tag{9}$$

This last result corresponds to the same choice of α than the previous case reported in Eq. (6), because the minimization problem is independent from r, and it expresses a degradation of the variance reduction effectiveness due to the presence of the coefficient $r/(1+r)$ which multiplies the correlation ρ^2. The origin of this reduction of efficiency of the method can be identified in the need for evaluating the LF control variates expected value term at the same time of the computation of the HF statistics. However, the parameter r controls the number of additional LF evaluations, therefore can be made arbitrary large for computational inexpensive LF models (and it is possible to recover the classical control variates results for LF with zero computational cost and $r \to \infty$).

In fact, in many practical applications the computational cost of a LF fidelity model can be order of magnitudes inferior to the corresponding HF one, but not negligible. Therefore the computational budget to allocate for the LF realizations must be taken into account. If the overall computational cost is written as

$$\mathcal{C}^{\mathrm{eq}} = \mathcal{C}^{\mathrm{HF}} + \mathcal{C}^{\mathrm{LF}}(1+r), \tag{10}$$

the optimal LF sample increment is

$$r = -1 + \sqrt{\frac{\rho^2}{1-\rho^2}w}, \tag{11}$$

where the ratio between the HF and LF computational cost is $w = \mathcal{C}^{\mathrm{HF}}/\mathcal{C}^{\mathrm{LF}}$. For convenience, we anticipated here this result that can be obtained solving a more general problem of the optimal allocation of samples across discretization (multilevel) and model fidelities (multifidelity). We postpone the description of the minimization problem to Sec. VI after having introduced how to define multilevel estimators which is the topic of the next section.

V. Multilevel estimators

A peculiar way of obtaining approximate models for the solution of PDEs is relaying on the numerical discretization. As discussed in the previous sections, the goal of the forward UQ in this work is to propagate

uncertain parameters through a code for a prescribed resolution level defined by the number M of its DOFs. We assume here that several resolution levels $\{M_\ell : \ell = 0, \dots, M\}$ with $M_0 < M_1 < \cdots < M_L \overset{\text{def}}{=} M$ are available, therefore we can exploit the linearity of the expected value operator and expanding in a telescopic sum (through levels) $\mathbb{E}\left[Q_M\right]$ as

$$\mathbb{E}\left[Q_M^{\text{HF}}\right] = \mathbb{E}\left[Q_{M_0}^{\text{HF}}\right] + \sum_{\ell=1}^{L} \mathbb{E}\left[Q_{M_\ell}^{\text{HF}} - Q_{M_{\ell-1}}^{\text{HF}}\right]. \tag{12}$$

We define a difference function Y_ℓ according to

$$Y_\ell^{\text{HF}} = \begin{cases} Q_{M_0}^{\text{HF}} & \text{if} \quad \ell = 0 \\ Q_{M_\ell}^{\text{HF}} - Q_{M_{\ell-1}}^{\text{HF}} & \text{if} \quad 0 < \ell \leq L, \end{cases} \tag{13}$$

hence the expected value $\mathbb{E}\left[Q_M^{\text{HF}}\right] = \sum_{\ell=0}^{L} \mathbb{E}\left[Y_\ell^{\text{HF}}\right]$. A multilevel MC estimator (MLMC) is obtained when a MC estimator is written for estimating at each level $\mathbb{E}\left[Y_\ell\right]$. We obtain

$$\hat{Q}_M^{\text{HF,ML}} = \sum_{\ell=0}^{L} \hat{Y}_{\ell,N_\ell}^{\text{HF,MC}} = \sum_{\ell=0}^{L} \frac{1}{N_\ell} \sum_{i=1}^{N_\ell} Y_\ell^{\text{HF},(i)}. \tag{14}$$

The multilevel MC estimator $\hat{Q}_M^{\text{HF,ML}}$ is unbiased and has a variance equal to

$$\mathbb{V}ar\left(\hat{Q}_M^{\text{HF,ML}}\right) = \sum_{\ell=0}^{L} N_\ell^{-1} \mathbb{V}ar\left(Y_\ell^{\text{HF}}\right). \tag{15}$$

The advantage of this formulation resides in two main differences with respect to the standard MC estimator. The first peculiarity of MLMC is the expansion of the variance over resolution levels, which does not contain covariance terms because on each level the MC estimator is, by definition, using independent sets of samples. The second difference with respect to MC is that the estimator, except for the coarsest $\ell = 0$ level, is written for the difference function Y_ℓ^{HF}. Hence, under the hypothesis that $Q_M^{\text{HF}} \to Q$ for $M \to \infty$, it is legitimate to assume $Y_\ell^{\text{HF}} \to 0$, therefore the variance contribution of the different resolution levels decreases with ℓ. The main advantage of this behavior for $\mathbb{V}ar\left(Y_\ell^{\text{HF}}\right)$ is that a target overall accuracy can be reached with decreasing allocation of samples N_ℓ for $\ell = 0, \dots, M$, *i.e.* the computational burden is shifted towards the coarser levels which are computationally cheaper to evaluate. The optimal sample allocation of the MLMC algorithm can be obtained minimizing the overall computational cost for a fixed target accuracy. In the hypothesis of a equal redistribution of the MSE between the bias term and the variance of the estimator, we can write

$$\mathbb{E}\left[\left(\hat{Q}_M^{\text{HF,ML}} - \mathbb{E}\left[Q_M^{\text{HF}}\right]\right)^2\right] = \sum_{\ell=0}^{L} \left(N_\ell^{\text{HF}}\right)^{-1} \mathbb{V}ar\left(Y_\ell^{\text{HF}}\right) + \left(\mathbb{E}\left[Q_M^{\text{HF}} - Q^{\text{HF}}\right]\right)^2 = \frac{\varepsilon^2}{2} + \frac{\varepsilon^2}{2} = \varepsilon^2, \tag{16}$$

indeed the MLMC algorithm guarantees the same deterministic bias of MC (see Eq.(2)) while reducing the variance of the estimator. For the multilevel method the overall computational cost is

$$\mathcal{C}(\hat{Q}_M^{\text{HF,ML}}) = \sum_{\ell=0}^{L} N_\ell^{\text{HF}}\, \mathcal{C}_\ell^{\text{HF}}, \tag{17}$$

with $\mathcal{C}_\ell^{\text{HF}}$ being the cost of the evaluation of Y_ℓ^{HF} (involving either one or two discretization evaluations). The computational cost Eq. (17) can be minimized under a variance constrain by means of a Lagrange multiplier λ. The minimization problem reads

$$\underset{N_\ell^{\text{HF}},\lambda}{\text{argmin}}(f), \quad \text{where} \quad f(N_\ell^{\text{HF}}, \lambda) = \sum_{\ell=0}^{L} N_\ell^{\text{HF}}\, \mathcal{C}_\ell^{\text{HF}} + \lambda \left(\sum_{\ell=0}^{L} \left(N_\ell^{\text{HF}}\right)^{-1} \mathbb{V}ar\left(Y_\ell^{\text{HF}}\right) - \varepsilon^2/2\right). \tag{18}$$

The optimal samples allocation (per level) as result of the minimization Eq. (18) is

$$N_\ell^{\text{HF}} = \frac{2}{\varepsilon^2} \left[\sum_{k=0}^{L} \left(\mathbb{V}ar\left(Y_k^{\text{HF}}\right) \mathcal{C}_k^{\text{HF}}\right)^{1/2}\right] \sqrt{\frac{\mathbb{V}ar\left(Y_\ell^{\text{HF}}\right)}{\mathcal{C}_\ell^{\text{HF}}}}. \tag{19}$$

VI. Multilevel-Multifidelity MLMF estimators

The multifidelity and multilevel approach presented in Sec. IV and V can be combined to achieve a larger variance reduction.[10,16,17] The main idea is to expand the expected value of the QoI over the resolution levels (multilevel) by targeting the difference function Y_ℓ^{HF} on each level. The MC estimator for each Y_ℓ^{HF} can be written by using a multifidelity control variate approach with estimated control means for the LF model, as described in Sec. IV.

More precisely, starting from Eq. (12), we can write

$$\begin{aligned}\mathbb{E}\left[Q_M^{\mathrm{HF}}\right] &= \mathbb{E}\left[Q_{M_0}^{\mathrm{HF}}\right] + \sum_{\ell=1}^{L} \mathbb{E}\left[Q_{M_\ell}^{\mathrm{HF}} - Q_{M_{\ell-1}}^{\mathrm{HF}}\right] \\ &= \sum_{\ell=0}^{L} \mathbb{E}\left[Y_{M_\ell}^{\mathrm{HF}}\right] \simeq \sum_{\ell=0}^{L} \hat{Y}_{M_\ell}^{\mathrm{HF,MC}} \\ &\simeq \sum_{\ell=0}^{L} \left(\hat{Y}_{M_\ell}^{\mathrm{HF,MC}} + \alpha_\ell \left(\hat{Y}_{M_\ell}^{\mathrm{LF,MC}} - \hat{\mathbb{E}}[Y_{M_\ell}^{\mathrm{LF}}]\right)\right).\end{aligned} \tag{20}$$

We seek for the optimal allocation of the samples N_ℓ^{HF} used to compute the MC estimator $\hat{Y}_{M_\ell}^{\mathrm{HF,MC}}$ and $\hat{Y}_{M_\ell}^{\mathrm{LF,MC}}$ and the optimal redistribution of the computational burden towards the LF model, which is defined by the set of independent samples $\Delta_\ell^{\mathrm{LF}}$ used to evaluate $\hat{\mathbb{E}}[Y_{M_\ell}^{\mathrm{LF}}]$ (see Eq. (8)).

On each level ℓ Eq. (9) holds, therefore we can write the full optimization problem Eq. (18) taking into account the MF variance reduction on each level

$$\underset{N_\ell^{\mathrm{HF}}, r_\ell, \lambda}{\operatorname{argmin}}(f), \quad \text{where} \quad f(N_\ell^{\mathrm{HF}}, r_\ell, \lambda) = \sum_{\ell=0}^{L} N_\ell^{\mathrm{HF}}\, \mathcal{C}_\ell^{\mathrm{eq}}(r_\ell) + \lambda \left(\sum_{\ell=0}^{L} \left(N_\ell^{\mathrm{HF}}\right)^{-1} \mathbb{V}ar\left(Y_\ell^{\mathrm{HF}}\right) \Lambda_\ell(r_\ell) - \varepsilon^2/2\right). \tag{21}$$

The function $\Lambda_\ell(r_\ell) = \left(1 - \frac{r_\ell}{1+r_\ell}\rho_\ell^2\right)$ in the previous equation measures the variance reduction achieved on each level by means of the LF control variates. The optimization problem Eq. (21) also differs from the one in Eq. (18) for the presence of the equivalent cost $\mathcal{C}_\ell^{\mathrm{eq}}$, induced by the LF evaluations, introduced in Eq. (10).

The solution of the optimization problem is obtained as

$$N_\ell^{\mathrm{HF}} = \frac{2}{\varepsilon^2}\left[\sum_{k=0}^{L_{\mathrm{HF}}} \left(\frac{\mathbb{V}ar\left(Y_k^{\mathrm{HF}}\right)\mathcal{C}_k^{\mathrm{HF}}}{1-\rho_\ell^2}\right)^{1/2} \Lambda_k(r_k)\right] \sqrt{(1-\rho_\ell^2)\,\frac{\mathbb{V}ar\left(Y_\ell^{\mathrm{HF}}\right)}{\mathcal{C}_\ell^{\mathrm{HF}}}}, \tag{22}$$

where the optimal redistribution of samples across LF and HF is given by

$$r_\ell = -1 + \sqrt{\frac{\rho_\ell^2}{1-\rho_\ell^2} w_\ell}, \tag{23}$$

as anticipated in Sec. IV.

On each level the sample allocation between LF and HF is controlled by r_ℓ which in turn depends on the correlation ρ_ℓ^2 and the computational cost ratio $w_\ell = \mathcal{C}_\ell^{\mathrm{HF}}/\mathcal{C}_\ell^{\mathrm{LF}}$. Useful information can be obtained if, for each level, we represent the optimal ratio r_ℓ as a function of these parameters. The optimal value for r_ℓ can also be used to compute the corresponding variance reduction $1 - \Lambda(r_\ell)$. In figure 1 it is possible to see that the algorithm requires an higher number of LF evaluations when both the correlation ρ_ℓ^2 and the cost ratio w_ℓ increase, whereas the variance reduction shows a higher dependence on ρ_ℓ^2 than w_ℓ. Therefore, a heavily biased LF model can still be useful to achieve a variance reduction (see for instance the numerical example[15]) if it is computationally cheaper that the HF model (high value of w_ℓ), however it needs to exhibit a non-negligible correlation ρ_ℓ^2 with the HF model.

In order to maximize the correlation between the LF and HF model a natural choice would be to update the LF improving its predictive capabilities. However, it is common for research efforts in a context of large

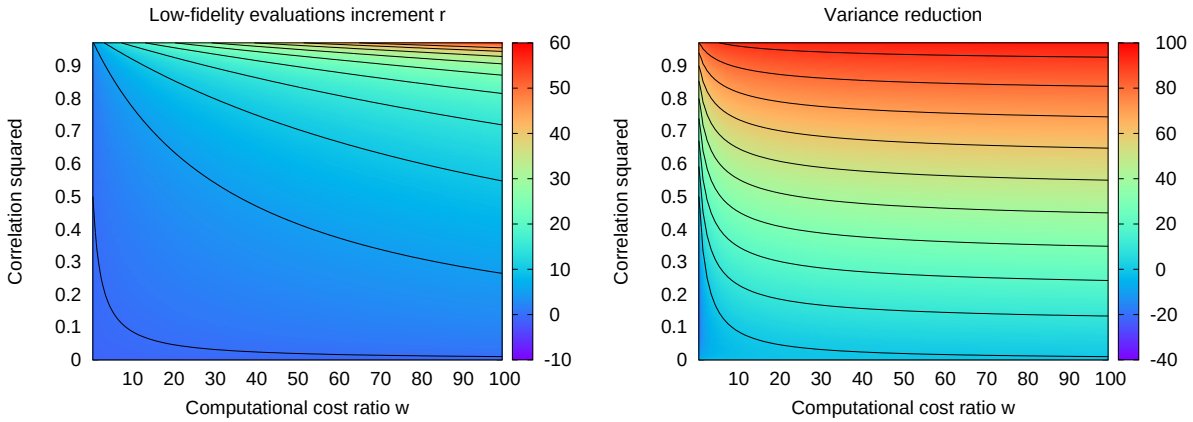

(a) Ratio r (b) Variance reduction (%)

Figure 1. Optimal LF additional evaluations ratio r and variance reduction (%). The contours line for the ratio r are provided between 0 and 45 with a step of 5, whereas for the variance reduction they are reported between 0 and 90% with step of 10%.

projects to have a certain degree of segregation between the application team and the UQ one. Therefore, updating the LF model could require few iterations and possibly a non-negligible effort needs to be invested in this task. In addition, the correlation evolution of ρ_ℓ with ℓ is fairly complicated to predict *a priori*. Indeed, it is possible to obtain LF models which are well correlated for coarser resolution levels where the solution is underresolved for the HF model too, and less correlated for higher resolution levels. Hence, in order to mitigate the possible lack of correlation other approaches are possible. For instance, if the HF model exhibits a certain degree of regularity and also a low-rank structure is present, this feature can be exploited to build a LF low-rank model which is expected to be well correlated for all the resolution levels. For more details the reader can refer to Ref. 11. Here, we present an alternative approach in which we try to maximize the correlation between Y_ℓ^{HF} and Y_ℓ^{LF} by using directly the quantities Q_ℓ^{HF} and Q_ℓ^{LF}. In fact, while the behavior of the correlation between discrepancies Y_ℓ is difficult to predict, we expect the quantities Q_ℓ to be better correlated. Eventually the CV is built level by level by seeking for a single additional optimal coefficient. We make use of the unbiased property on the multifidelity control variate (Sec. IV) to build a control variate which is based on LF realizations but is not obtained as difference between two adjacent resolution levels. We instead seek for the optimal generalized difference function $\mathring{Y}_\ell^{\mathrm{LF}}$ given by

$$\mathring{Y}_\ell^{\mathrm{LF}} = \gamma_\ell Q_\ell^{\mathrm{LF}} - Q_{\ell-1}^{\mathrm{LF}}, \tag{24}$$

where the additional coefficient γ_ℓ (to be determined) offers an additional degree-of-freedom to obtain a higher correlation.

Equation (25) can be re-written with the new control variates $\mathring{Y}_\ell^{\mathrm{LF}}$

$$\mathbb{E}\left[Q_M^{\mathrm{HF}}\right] \simeq \sum_{\ell=0}^{L} \left(\hat{Y}_{M_\ell}^{\mathrm{HF,MC}} + \alpha_\ell \left(\mathring{Y}_\ell^{\mathrm{LF,MC}} - \hat{\mathbb{E}}[\mathring{Y}_\ell^{\mathrm{LF}}] \right) \right), \tag{25}$$

where the new correlation between $\hat{Y}_{M_\ell}^{\mathrm{HF}}$ and $\mathring{Y}_\ell^{\mathrm{LF}}$ is now a function of γ_ℓ as

$$\mathring{\rho}_\ell^2 = \mathring{\rho}_\ell^2(\gamma_\ell) = \rho_\ell^2 \frac{\theta_\ell^2}{\tau_\ell}, \tag{26}$$

with

$$\begin{aligned} \theta_\ell &= \theta_\ell(\gamma_\ell) = \frac{\mathrm{Cov}\left(Y_\ell^{\mathrm{LF}}, \mathring{Y}_\ell^{\mathrm{LF}}\right)}{\mathrm{Cov}\left(Y_\ell^{\mathrm{LF}}, Y_\ell^{\mathrm{LF}}\right)} \\ \tau_\ell &= \tau_\ell(\gamma_\ell) = \frac{\mathbb{V}ar\left(\mathring{Y}_\ell^{\mathrm{LF}}\right)}{\mathbb{V}ar\left(Y_\ell^{\mathrm{LF}}\right)}. \end{aligned} \tag{27}$$

We seek for the optimal γ_ℓ coefficient which maximizes the correlation $\mathring{\rho}_\ell^2$ that corresponds to the maximization of the function θ_ℓ^2/τ_ℓ and, finally to the following formulation

$$\begin{aligned}\underset{\gamma_\ell}{\text{argmax}}\left(\mathcal{F}(\gamma_\ell)\right), \quad \text{where} \quad \mathcal{F}(\gamma_\ell) &\overset{\text{def}}{=} \frac{\left(\text{Cov}\left(Y_\ell^{\text{HF}}, \mathring{Y}_\ell^{\text{LF}}\right)\right)^2}{\mathbb{V}ar\left(\mathring{Y}_\ell^{\text{LF}}\right)} \\ &= \frac{\left[\gamma_\ell \text{Cov}\left(Y_\ell^{\text{HF}}, Q_\ell^{\text{LF}}\right) - \text{Cov}\left(Y_\ell^{\text{HF}}, Q_{\ell-1}^{\text{LF}}\right)\right]^2}{\gamma_\ell^2 \mathbb{V}ar\left(Q_\ell^{\text{LF}}\right) + \mathbb{V}ar\left(Q_{\ell-1}^{\text{LF}}\right) - 2\gamma_\ell \text{Cov}\left(Q_\ell^{\text{LF}}, Q_{\ell-1}^{\text{LF}}\right)},\end{aligned} \tag{28}$$

where its analytical solution is given by

$$\gamma_\ell = \frac{\text{Cov}\left(Y_\ell^{\text{HF}}, Q_{\ell-1}^{\text{LF}}\right)\text{Cov}\left(Q_\ell^{\text{LF}}, Q_{\ell-1}^{\text{LF}}\right) - \mathbb{V}ar\left(Q_{\ell-1}^{\text{LF}}\right)\text{Cov}\left(Y_\ell^{\text{HF}}, Q_\ell^{\text{LF}}\right)}{\mathbb{V}ar\left(Q_\ell^{\text{LF}}\right)\text{Cov}\left(Y_\ell^{\text{HF}}, Q_{\ell-1}^{\text{LF}}\right) - \text{Cov}\left(Y_\ell^{\text{HF}}, Q_\ell^{\text{LF}}\right)\text{Cov}\left(Q_\ell^{\text{LF}}, Q_{\ell-1}^{\text{LF}}\right)}. \tag{29}$$

Eventually, the full solution, in term of optimal allocation of samples across discretization levels and model fidelities, is given by

$$\begin{aligned} r_\ell &= -1 + \sqrt{\frac{\mathring{\rho}_{HL}^2}{1-\mathring{\rho}_{HL}^2} w_\ell}, \quad \text{where} \quad w_\ell = \mathcal{C}_\ell^{\text{HF}}/\mathcal{C}_\ell^{\text{LF}} \\ \Lambda_\ell &= 1 - \mathring{\rho}_{HL}^2 \frac{r_\ell}{1+r_\ell} \\ N_\ell^{\text{HF}} &= \frac{2}{\varepsilon^2}\left[\sum_{k=0}^{L_{\text{HF}}} \left(\frac{\mathbb{V}ar\left(Y_k^{\text{HF}}\right)\mathcal{C}_k^{\text{HF}}}{1-\mathring{\rho}_{HL}^2}\right)^{1/2} \Lambda_k(r_k)\right] \sqrt{\left(1-\mathring{\rho}_{HL}^2\right)\frac{\mathbb{V}ar\left(Y_\ell^{\text{HF}}\right)}{\mathcal{C}_\ell^{\text{HF}}}} \end{aligned}$$

In the following, whenever we present numerical results for the MLMF estimator we will always assume to use this latter formulation with $\mathring{\rho}_\ell$ which, in separate studies, demonstrated to achieve better performances than the one based on ρ_ℓ.

VII. Some practical considerations

In the previous sections we described how to efficiently define multifidelity, multilevel and multilevel-multifidelity MC statistical estimators. However, from a practical standpoint additional details should be clarified in order to apply the methods described above. Indeed, two main difficulties arise during the deployment for large scale engineering applications. First, in many applicatins the UQ step should take into account a vector of quantities of interest not only a scalar QoI. Moreover, the computational budget available might be insufficient to reach the optimal allocation of samples N_ℓ^{HF} provided an arbitrary tolerance ε. In the following we describe possible practical solutions to these two issues that we resorted in this work to obtain the numerical results reported in Sec. IX. For all the numerical computations we also use the DAKOTA[4] software which features an implementation of the algorithms described here.

VII.A. Extension to multiple QoIs

All the estimators described in the previous sections are based on a scalar QoI. This approach impacts the optimal allocation r between model fidelitites, Eq. (11), in the multifidelity estimator, and the sample allocation N_ℓ^{HF} in both the multilevel, Eq.(19), and multilevel-multifidelity, Eq.(22). For the multifidelity estimator the distinction between the case with a scalar or vector of QoIs resides in the selection of the correlation. Instead, to build the multilevel operator it is also necessary to know the variance for the difference function Y_ℓ^{HF} (of a scalar QoI). The multilevel-multifidelity estimator, being the combination of the two ones mentioned above, requires either a scalar correlation and variance.

In principle, for the multilevel based estimator the variance for each QoI can be constrained by a separate Lagrange multiplier, however this approach poses some mathematical difficulties since it can lead to the activation of distinct Lagrange multipliers, *i.e.* constraints, on each level. To overcome this issue we use the following heuristic procedure: for both the ratio r_ℓ and the correlation squared ρ_ℓ^2 we compute the average

value across QoIs. Afterward, we use these two values to evaluate the corresponding variance reduction $\tilde{\Lambda}_\ell = \Lambda_\ell(r_\ell, \rho_\ell^2)$ as a separate function of correlation and low-fidelity sample increment r_ℓ. Moreover, the variance on each level is determined as the aggregation of the variances of each QoI. This assumption would be correct only in case of independent QoIs, therefore it is only an approximation for the general case of correlated QoIs. Our experience with different test cases reveals that an alternative choice would consist in evaluating a weighted average of the correlations of the QoI based on the contribution of each QoI to the overall variance (per level). However, this refinement of the current approach is the subject of additional investigations, therefore in this work we adopt the heuristic strategy described above and based on the (un-weighted) average.

VII.B. Computational constrained budget

In many practical situations the computational budget would allow for only an handful of realizations for the HF model at the finest resolution. Therefore, it could be challenging to obtain the optimal sample allocation dictated by N_ℓ^{HF} for an arbitrary tolerance ε. One example of this kind of situation is described later on for the SCRAMJET problem (Sec. VIII.B).

We propose the following algorithm to determine the optimal allocation per level for the general case of the multilevel-multifidelity estimator when the maximum number of samples at level $\ell = L$ for the HF model is assigned *a priori*. We first note that the ratio between the optimal number of samples per level for HF is independent from the target accuracy ε

$$N_\ell^{\mathrm{HF}} / N_{\ell-1}^{\mathrm{HF}} = \sqrt{\frac{1-\rho_\ell^2}{1-\rho_{\ell-1}^2} \frac{\mathbb{V}ar\left(Y_\ell^{\mathrm{HF}}\right)}{\mathbb{V}ar\left(Y_{\ell-1}^{\mathrm{HF}}\right)} \frac{\mathcal{C}_{\ell-1}^{\mathrm{HF}}}{\mathcal{C}_\ell^{\mathrm{HF}}}}, \tag{30}$$

therefore it is possible to define the optimal sequence of ratios ω as

$$\omega = \left(\omega_1 = \frac{N_1^{\mathrm{HF}}}{N_0^{\mathrm{HF}}}, \omega_2 = \frac{N_2^{\mathrm{HF}}}{N_1^{\mathrm{HF}}}, \dots \omega_{L-1} = \frac{N_{L-1}^{\mathrm{HF}}}{N_{L-2}^{\mathrm{HF}}}, \omega_L = \frac{N_L^{\mathrm{HF}}}{N_{L-1}^{\mathrm{HF}}} \right).$$

If the computational budget allows a maximum of $N_{\mathrm{target}}^{\mathrm{HF}}$ evaluations, the optimal allocation across levels would be

$$\hat{N}_\ell^{\mathrm{HF}} = N_{\mathrm{target}}^{\mathrm{HF}} \Big/ \left(\prod_{q=0}^{L-\ell-1} \omega_{L-q} \right). \tag{31}$$

Eventually, the optimal cost redistribution between model fidelity is obtained on each level as

$$N_\ell^{\mathrm{LF}} = (1 + r_\ell)\, \hat{N}_\ell^{\mathrm{HF}} \tag{32}$$

VII.C. A possible practical implementation

We report here the steps needed for a possible implementation of the multilevel-multifidelity algorithm whereas the multilevel and multifidelity estimators can be obtained executing only a subset of its operations.

1 Pilot runs for the LF:

- Evaluation of $\mathbb{E}\left[Q_\ell^{\mathrm{LF}}\right]$ and $\mathbb{E}\left[Q_{\ell-1}^{\mathrm{LF}}\right] \rightarrow \mathbb{E}\left[Y_\ell^{\mathrm{LF}}\right] = \mathbb{E}\left[Q_\ell^{\mathrm{LF}}\right] - \mathbb{E}\left[Q_{\ell-1}^{\mathrm{LF}}\right]$
- Evaluation of $\mathbb{V}ar\left(Q_\ell^{\mathrm{LF}}\right), \mathbb{V}ar\left(Q_{\ell-1}^{\mathrm{LF}}\right)$, and $\mathrm{Cov}\left(Q_\ell^{\mathrm{LF}}, Q_{\ell-1}^{\mathrm{LF}}\right)$

2 Pilot runs for HF (same LF sample realizations):

- Evaluation of $\mathrm{Cov}\left(Y_\ell^{\mathrm{HF}}, Q_\ell^{\mathrm{LF}}\right)$, and $\mathrm{Cov}\left(Y_\ell^{\mathrm{HF}}, Q_{\ell-1}^{\mathrm{LF}}\right)$
- Evaluation of $\mathrm{Cov}\left(Y_\ell^{\mathrm{HF}}, Y_\ell^{\mathrm{LF}}\right) = \mathrm{Cov}\left(Y_\ell^{\mathrm{HF}}, Q_\ell^{\mathrm{LF}}\right) - \mathrm{Cov}\left(Y_\ell^{\mathrm{HF}}, Q_{\ell-1}^{\mathrm{LF}}\right)$
- Evaluation of $r_\ell = \mathrm{Cov}\left(Y_\ell^{\mathrm{HF}}, Y_\ell^{\mathrm{LF}}\right) / \left(\mathbb{V}ar^{1/2}\left(Y_\ell^{\mathrm{HF}}\right) \mathbb{V}ar^{1/2}\left(Y_\ell^{\mathrm{LF}}\right)\right)$

3 Computations of LF-HF coupling parameters:

- Optimal ratio $\hat{\gamma}_\ell$
- Covariance ratio θ_ℓ
- Variance ratio τ_ℓ
- Enhanced correlation $\mathring{\rho}^2_\ell$

4 Optimal multilevel allocation ratios ω

5 Multilevel budget-constrained allocation $\hat{N}^{\mathrm{HF}}_\ell$

6 Optimal cost repartition between HF and LF $N^{\mathrm{LF}}_\ell = (1 + r_\ell)\,\hat{N}^{\mathrm{HF}}_\ell$

VIII. Applications demonstrations

In this section we furnish a brief description of the two applications we use to demonstrate the efficiency of the multilevel-mulifidelity estimator when compared to MC and multilevel estimators. The first problem is a thermo-aero-structural analysis of a nozzle device in cruise condition subject to uncertainties in operative conditions and manufacturing properties. The second example is derived from a SCRAMJET HIFiRE and it focus on its region of the primary injector. In this manuscript, for the sake of brevity, only the details needed for the formulation of the UQ forward problem are described and the reader is invited to refer to Alonso *et al.*[1] for a more detailed description of the nozzle case and to Vane *et al.*,[32] and Huan *et al.*[20] for a more in depth discussion of the numerical approach and the SCRAMJET configuration.

VIII.A. Northrop Grumman X-47B inspired nozzle design

In the context of the DARPA funded project SEQUOIA we are interested in the design under uncertainties of devices that involve aero-structural-thermal interactions in advanced aerospace vehicles across a broad spectrum of the speed regime. A problem of interest is a nozzle for advanced vehicles such as the Northrop Grumman UCAS X-47B showed in figure 2. Geometry data and estimated performances of the X-47B are reported in table 1[12]. One of the fundamental step of the design under uncertainties is the ability to efficiently propagate uncertainty through the numerical code.

(a) X47B UCAS (b) Nozzle close-up

Figure 2. Northrop Grumman X-47B UCAS and close up of its nozzle.[25]

The X47B is powered by a Pratt & Whitney F100-PW-220 turbofan engine without after-burning capabilities. A simplified engine model simulator is adopted[12,13,14] to generate the inlet condition of the nozzle. The baseline geometry of the nozzle is reported in figure 3(a). Moreover, during the normal operative conditions the nozzle structure is exposed to both thermal and mechanical loading. Therefore we decided to model the structure of the device using a two-layer array (see figure 3(b)), namely a thermal and a loading layer, placed internally and externally, respectively.

For this problem, we present a preliminary UQ analysis of the nozzle device for the cruise condition of the vehicle. We decided to rely on axisymmetric Euler computations for the internal flow of the nozzle, with input conditions generated by the engine model of F100-PW-220. The SU2[9] CFD code is used to solve the

Parameter	Value
Span (m)	18.93
Empty weight (Kg)	$6,350$
TOGW (Kg)	$20,215$
Payload (Kg)	$2,040$
$L/D\|_{\text{cruise}}$	12.62-15.58
Cruise Mach	0.45
Top speed	high subsonic
Range (nm)	$2,100$
Endurance (hr)	6
Service Ceiling (ft)	$40,000$

Table 1. Geometry and estimated performances for X-47B.[12]

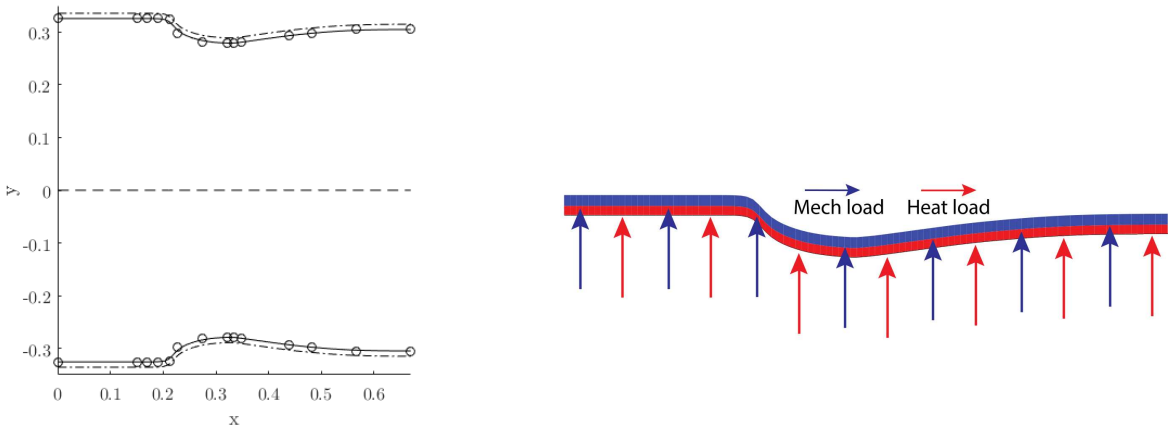

(a) Nozzle baseline geometry (in meters)

(b) Nozzle thermal-structural model

Figure 3. Baseline nozzle geometry (a) and its thermal-structural layer layout (b). The thermal and load layer are placed internally and externally, respectively.

internal flow and generate the temperature and pressure profile along the nozzle wall. An array of SU2 flow realizations in the presence of different nozzle geometries is reported in figure 4 as an example.

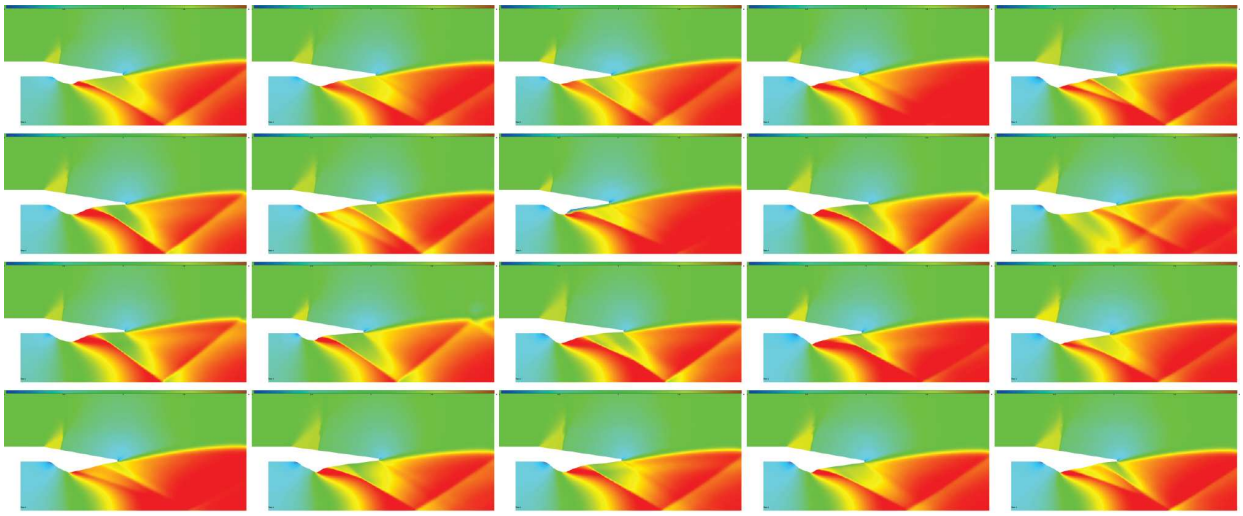

Figure 4. Example of Euler computations for different nozzle geometries.

Afterward, the temperature profile is provided to a thermal FEM solver which computes the temperature distribution over the entire volume, *i.e.* the nozzle structure. Finally, the pressure distribution at the wall and the temperature field inside the structure serve as input conditions for a FEM structural solver which computes the stresses distributions in the structure. An example of the thermal field and mechanical stresses is reported in figure 5. The procedure described so far represents the high-fidelity model we adopted for our simulations.

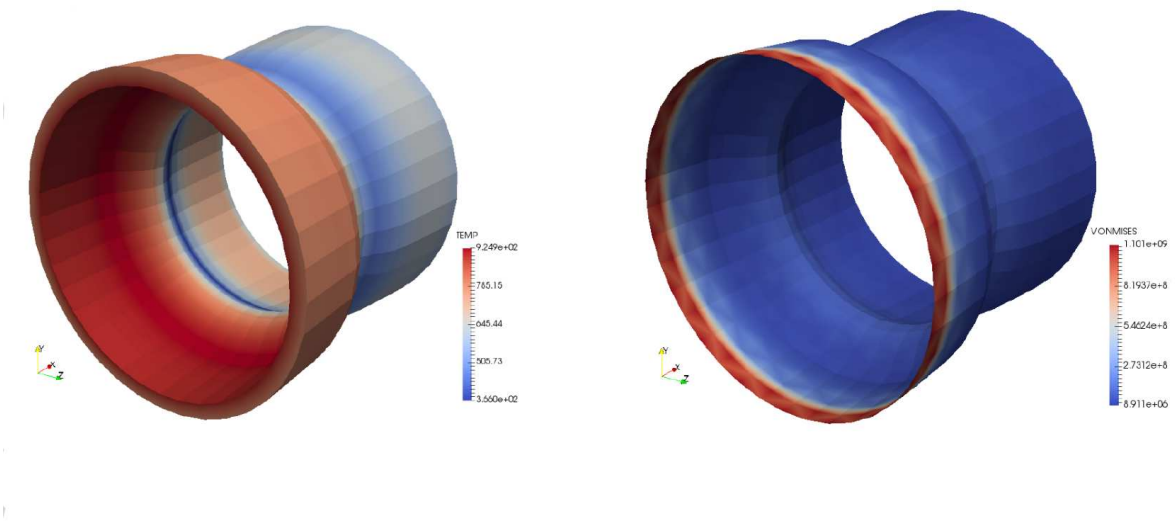

Figure 5. Example of temperature field and von Mises stresses inside the nozzle structure as a result of the FEM analyses.

For a preliminary analysis, we are interested in the performances of the nozzle in term of generated thrust and two reliability measures that we identified in the maximum thermal and mechanical stresses. In order to generate a low-fidelity approximation two different approaches are pursued. Initially a simplified non ideal one dimensional model has been adopted for the computation of the flow, thermal and mechanical stress, while the engine model is identical for the LF and HF models. In particular, this low-fidelity model is obtained performing the following operations[13]

- Ideal (adiabatic and frictionless) nozzle equations are solved to determine the flow conditions;

- Quasi-1D (area-averaged) equations are integrated to compute the actual flow solution and temperature distribution;
- A heat transfer calculation is carried out in the transverse direction by means of thermal resistances. The model estimates convection and conduction from the nozzle fluid to the nozzle wall, conduction through the nozzle wall, and sum of convection, conduction and radiation from the exterior nozzle wall to the environment.
- Stagnation temperature as well as the wall heat flux along the nozzle are determined;
- The coefficient of friction is computed;
- Mach number (dependent on stagnation temperature and friction coefficient) is updated and few iterations are performed until convergence.

To evaluate the stresses a simple hoop model is adopted for the mechanical part, while the thermal stress in a cylinder are computed in each axial section of the nozzle. In summary, this low-fidelity model differs from the high-fidelity one for the following aspects: the Euler flow solution is replaced by a non-ideal one dimensional model and the FEM thermal and structural analyses by a thermal resistance model and hoop stresses, respectively.

The low-fidelity model described above demonstrated to be able to predict accurate values for the thrust, but it produces low correlated values for the stresses with respect to the HF one (see Sec. IX.A). Therefore, we completed a full iteration between the UQ and application teams which led to an updated low-fidelity model. In particular, we replaced the thermal and mechanical computations with a FEM solution, identical to the HF model. This choice is motivated by the low-correlation of the stresses, but also by the repartition of the computational cost between the fluid and thermo-structural part. Indeed, since the FEM solutions represent a negligible cost compared to the Euler computation, adopting the FEM solutions for the LF is expected to increase the quality of the stresses prediction with a negligible increase of the computational cost (that we will not consider in this work).

For both the low-fidelity models we will not consider the presence of different resolution levels. Therefore, the low-fidelity model is paired to the coarsest resolution level of the HF model to obtain a multifidelity CV, while other two HF resolutions are adopted in order to build the multilevel part of the estimator. Further details regarding the computational settings are provided in Sec. IX.A.

VIII.B. HIFiRE SCRAMJET engine

Funded by DARPA, within the ScramjetUQ project we are interested in demonstrating advanced UQ algorithms and strategies in multiphysics computations of a supersonic turbulent spray combustion SCRAMJET engine. A SCRAMJET engine is a device which relies on its high-velocity to compress the incoming air before combustion, however without reducing the air velocity to subsonic conditions before the combustion as instead it happens in a RAMJET engine. A cartoon sketching a SCRAMJET during its flight is reported in figure 6.

This problem is particularly challenging for UQ for its substantial computational cost and its complex physics nature: compressible gasdynamics, shock waves, multiphase flow, real-gas effects, turbulence and combustion phenomena are present. The overall goal of our research is to study the HIFiRE SCRAMJET configuration.[6,21] HIFiRE is a cavity-based hydrocarbon-fueled dual mode SCRAMJET that can control the transition between the subsonic combustion mode (RAMJET) to the supersonic mode (SCRAMJET) through timing of the injectors. An experimental setup is available and is reported in figure 7(left). For the preliminary UQ propagation study reported in this manuscript we consider a unit problem that focuses on the subdomain of primary injection. The focus is on the interaction between the fuel jet and the supersonic air cross flow without combustion. The unit problem is reported in figure 7(right).

The computations are carried out using the RAPTOR code[28] which is a CFD code designed for solving large eddy simulations (LES) for combustion problems in complex geometries. An array of realizations for an increasing levels of resolution is reported in figure 8 as an example. High-fidelity realizations are obtained by means of three-dimensional LES computations.

For this problem we choose 2D numerical realizations as the low-fidelity model. Unlike the nozzle problem, we employ the same discretization levels for both the LF and HF, therefore all the HF levels used to build the multilevel estimator are subject to LF CV. The details of the choice of the resolution levels are furnished

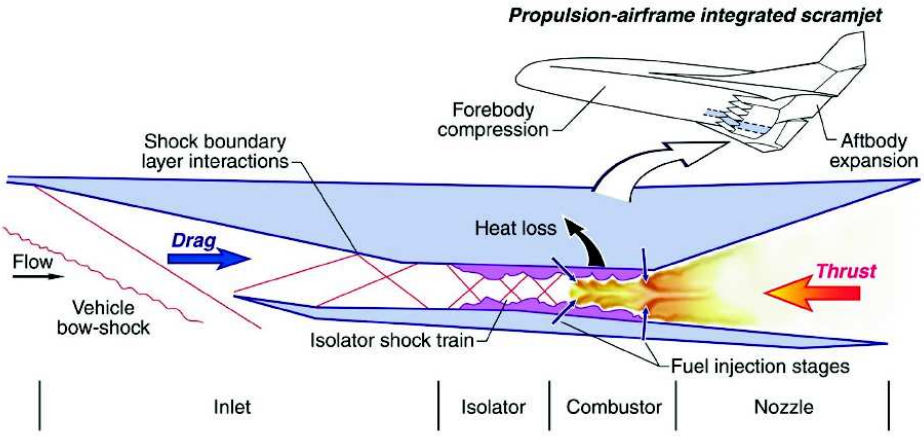

Figure 6. Cartoon of a SCRAMJET engine during flight conditions.

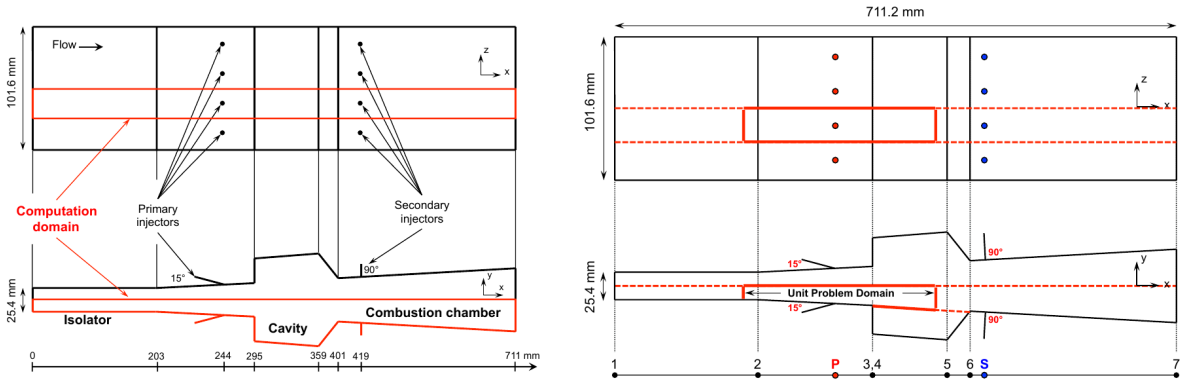

Figure 7. Experimental full combustor geometry (left) and the unit problem domain (right).

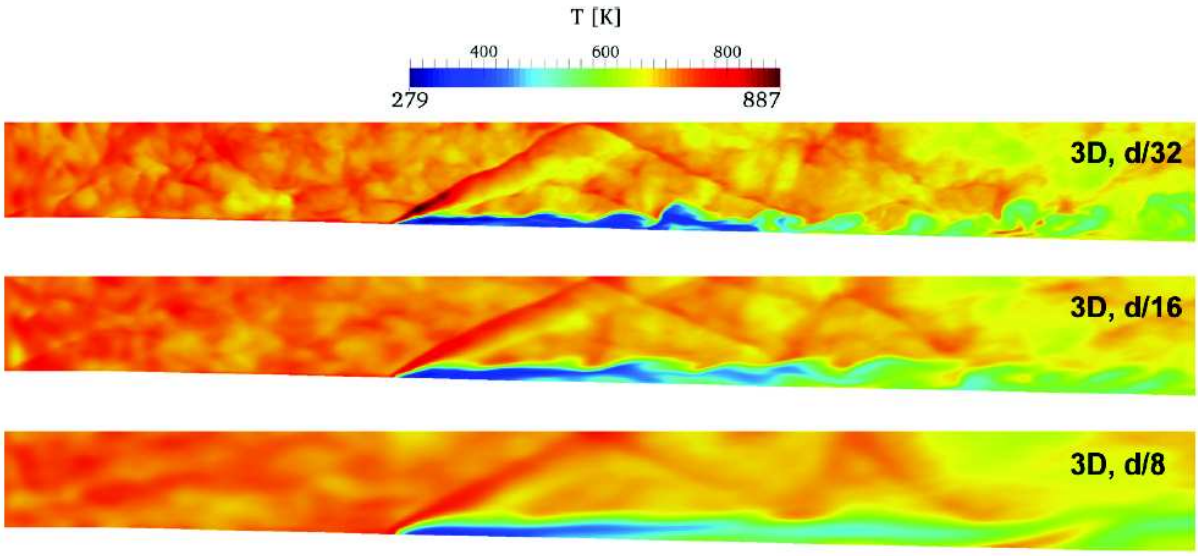

Figure 8. Instantaneous temperature field over resolutions. Numerical resolutions are labeled in term of the number of cells used to represent the diameter of the injector, namely $d/8$, $d/16$, and $d/32$.

in Sec. IX.B. We are interested in five different QoIs, namely (transverse direction) mean stagnation pressure $P_{0,mean}$, mean stagnation pressure RMS (RMS is over time) $P_{0,rms,mean}$, mean Mach number M_{mean}, mean turbulent kinetic energy TKE_{mean}, and mean scalar dissipation χ_{mean}. These QoIs are relevant for the unit problem and representative for other variables output by the LES. All QoIs are computed along a prescribed spatial location corresponding to a plane located at distance $x/d = 100$ from the inlet.

IX. Numerical results

IX.A. Aero-thermo-structural nozzle performances analysis

The aero-thermo-structural UQ analysis for the nozzle problem described in Sec. VIII.A is presented in the following. We consider three QoIs, namely the thrust generated, the mechanical and thermal maximum stresses. For this study we consider the propagation of a vector of 15 uniform and independent random parameters which includes operative conditions, material properties and geometrical parameters. The random parameters and their ranges are reported in table 2. The geometry of the nozzle is parametrized by using four base splines (B-spline) coefficients for the internal and external part of the nozzle structure (which is axisymmetric, see figure 3). The multilevel estimators are built using three meshes for the Euler solution which are reported as reference in figure 9.

Parameter	Range
Inlet stagnation temperature [K]	897.75-992.25
Atmospheric Temperature [K]	248.9-275.1
Inlet stagnation pressure [Pa]	216,000-264,000
Atmospheric Pressure [Pa]	57,000-63,000
Thermal conductivity [W/m K]	8.064-9.856
Elastic modulus [Pa]	7.38e10-9.02e10
Thermal expansion coefficient [1/K]	1.8e-6-2.2e-6
lower Bspline 1 [-]	0.005-0.03
lower Bspline 2 [-]	0.005-0.03
lower Bspline 3 [-]	0.005-0.03
lower Bspline 4 [-]	0.005-0.03
upper Bspline 1 [-]	0.005 -0.03
upper Bspline 2 [-]	0.005-0.03
upper Bspline 3 [-]	0.005-0.03
upper Bspline 4 [-]	0.005-0.03

Table 2. Uncertain parameters for the nozzle problem.

Moreover, the number of triangles of each mesh is reported in table 3 as reference. The solution on each mesh lead to a computational cost which is reported in table 4. The computational cost is normalized with respect to the HF fine solution. The ratio w between the computational cost of the HF and LF coarse is equal to 3.31.

	Triangles
Coarse	6,119
Medium	29,025
Fine	142,124

Table 3. Number of triangles for each mesh used to compute the Euler solution for the nozzle problem.

We generate a set of 20 pilot samples across all resolution levels and fidelities, where both the low-fidelity model are paired with the coarsest level of HF. In table 5 the results for the correlation of the two low-fidelity models are reported. It appears evident that the low-fidelity model based on the simplified thermal and mechanical stresses computation is unable to achieve a significant correlation for the stresses, whereas the updated model reaches a very high correlation for all the QoIs.

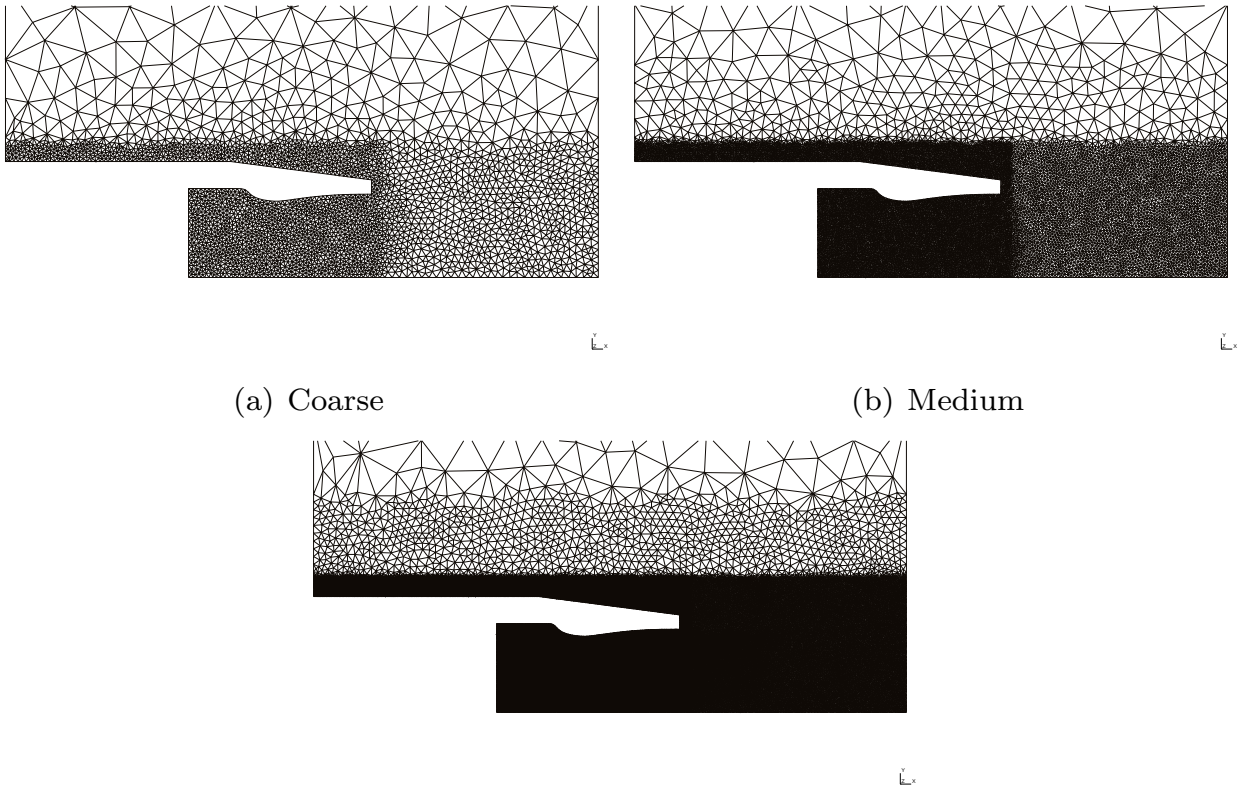

(a) Coarse (b) Medium

(c) Fine

Figure 9. Close up of the meshes used to define the multilevel discretizations for the nozzle problem in SU2.

	LF	HF
Coarse	0.016	0.053
Medium	N/A	0.253
Fine	N/A	1.0

Table 4. Computational cost for the LF and HF models. The two low-fidelity models have a negligible computational cost difference, therefore they are assumed to have the same cost.

The lack of correlation of the simplified low-fidelity model produces a non-optimal allocation of samples between fidelities that can be seen in table 6. In table 6, for different values of the normalized accuracy ε (where ε_0 is the accuracy attained by a multilevel estimator built using only the pilot samples), we report the sample allocations for all the discretization levels and fidelities. It is evident, for instance comparing the sample allocation for $\varepsilon^2/\varepsilon_0^2 = 0.001$, that the low correlation of the stresses forces the algorithm to a number of HF simulations at coarse level which is one order of magnitude higher than the correspondent value for the MLMF estimator based on the updated low-fidelity model.

For the value of accuracy $\varepsilon^2/\varepsilon_0^2 = 0.001$ we report in table 7 the values of correlations attained and the corresponding variance reduction for each QoI.

The results in term of total computational cost for different values of $\varepsilon/\varepsilon_0$ are reported in figure 10. For comparison, the results corresponding to the equivalent MC and MLMC estimators are also shown. For the simplified LF model the MLMC outperforms the MLMF estimator. The reason can be identified in the uneven behavior of the correlation across the QoIs. A low correlation is associated to the stresses, but a much higher correlation (0.99) is associated to the thrust. Therefore, the equivalent correlation we use to drive the algorithm, which is the average of all the correlations, is still high enough to allow for LF computations even if the overall variance reduction can be obtained only for the thrust. If the metric of interest is the aggregation of the variance, then the contribution of the thrust is less significant than the variances of the stresses. The order of magnitude for the standard deviation of the thrust is of $\mathcal{O}(10^3)$, while is of $\mathcal{O}(10^7)$

	1D flow + simplified stress analysis	1D flow + FEM
Thrust	9.98e-01	9.98e-01
Mechanical Stress	2.23e-02	9.66e-01
Thermal Stress	3.96e-01	9.93e-01

Table 5. Correlation for the two low-fidelity models for the nozzle problem. The first low-fidelity model is obtained by coupling a 1D non-ideal solver for the fluid part and a thermal resistances and hoop model for the mechanical and thermal stresses, respectively. The updated LF model is obtained replacing the stress simplified computations with the FEM analyses. This correlation values correspond to the accuracy $\varepsilon^2/\varepsilon_0^2 = 0.01$.

Accuracy ($\varepsilon^2/\varepsilon_0^2$)	LF	HF			LF (updated)	MF		
	Coarse	Coarse	Medium	Fine	Coarse	Coarse	Medium	Fine
0.1	N/A	N/A	N/A	N/A	404	20	20	20
0.01	21,143	1,757	20	20	3,091	177	31	20
0.003	69,580	5,775	36	20	N/A	N/A	N/A	N/A
0.001	212,828	17,715	109	34	32,433	1,773	314	20

Table 6. MLMF sample profile for the two LF models and HF as function of the normalized accuracy $\varepsilon^2/\varepsilon_0^2$.

	LF		LF (updated)	
	correlation	Variance reduction [%]	correlation	Variance reduction [%]
Thrust	0.997	91.42	0.996	94.2
Mechanical Stress	2.23e-2	2.12e-3	0.944	89.2
Thermal Stress	0.396	12.81	0.987	93.4

Table 7. Correlations and variance reduction for the nozzle problem for $\varepsilon^2/\varepsilon_0^2 = 0.001$. The data are relative to the coarse level which is the only one in which the multifidelity CV is employed for this problem.

for both the thermal and mechanical stresses. A partial solution to this imbalance would consist in the evaluation of a weighted average of the correlation (as anticipated in Sec. VII.A) with respect to the overall variance. In this latter case the MLMF would be able to recognize that the LF is not correlated enough with the HF model to bring a benefit in term of aggregate variance reduction and therefore the MLMF estimator would coincide with MLMC, *i.e.* no LF evaluations are required. For the updated LF model the correlation is almost evenly distributed across QoIs, therefore the MLMF is achieving a better performance than both MC and MLMC without any particular treatment to compute the equivalent correlation across multiple QoIs.

In figure 10 it is also possible to note that the number of pilot runs (20) performed on each level for the two models resulted to be too high with respect to the final accuracy required. Indeed, the optimal allocation is always obtained without requiring additional evaluations at the finest HF level.

IX.B. Scramjet

For the scramjet problem described in Sec. VIII.B we selected five QoIs for which we target the aggregated variance for the optimal sample allocation. We perform the propagation of 24 uncertain variables which are reported along with their ranges in table 8.

Two discretization levels are used for the HF model, namely with 8 ($d/8$) or 16 ($d/16$) cells to discretize the injector diameter. The low fidelity model is constituted by 2D LES simulations and the computational cost normalized in term of a HF 3D run is reported in table 9.

For this application the computational cost for the finest HF level is extremely high with respect to all the other levels and fidelity. The ratios w_ℓ are 204 for $\ell = 0$, and 77 for $\ell = 1$. Therefore we had to constrain the number of HF runs as described in Sec. VII.B. In particular we initialized the algorithm requiring 46 and 12 realizations on $d/8$ and $d/16$, respectively for each model. Among them some runs failed to converge, therefore the effective number of pilot runs was 39 and 9. Afterward, we constrained the algorithm to target the most efficient sample allocation without requiring additional 3D $d/16$ realizations. The optimal allocation led to the results reported in table 10 which corresponds to $\varepsilon^2/\varepsilon_0^2 = 0.045$.

Parameter	Symbol	Range
Inflow boundary conditions		
Inlet		
Stagnation pressure	$p_{0,i}$	1.48 MPa $\pm$ 5%
Stagnation temperature	$T_{0,i}$	1550 K $\pm$ 5%
Mach number	M_i	2.51 $\pm$ 10%
Turbulence intensity	$I_i = u_i^{'}/U_i$	[0.0 $-$ 0.05]
Turbulence intensity ratio	$I_r = v_i^{'}/u_i^{'}$	1.0
Turbulence length scale	L_i	[0.0 $-$ 8.0]mm
Boundary layer thickness	δ_i	[2.0 $-$ 6.0]mm
Fuel injection $(36\%CH_4, 64\%C_2H_4)$		
Mass flux	$\dot{m}_f$	7.37×10^{-3} kg/s $\pm$ 10%
Static Temperature	T_f	300.0 K $\pm$ 5%
Mach Number	M_f	1.0 $\pm$ 5%
Turbulence intensity	$I_f = u_f^{'}/U_f$	[0.025 $-$ 0.075]
Turbulence length scale	L_f	[0.02 $-$ 1.0] mm
Wall boundary conditions		
Wall Temperature	T_w	Profile from KLE Expansion (10 params)
Turbulence model parameters		
Static Smagorinsky		
Modified Smagorinsky constant	C_R	$[0.01 - 0.016]$
Turbulent Prandtl number	Pr_t	$[0.5 - 1.7]$
Turbulent Schmidt number	Sc_t	$[0.5 - 1.7]$

Table 8. Summary of the uncertain parameters for the SCRAMJET problem.

	2D	3D
$d/8$	5E-4	0.11
$d/16$	0.014	1

Table 9. Computational cost for the LF and HF models as function of resolution (normalized w.r.t. a single 3D fine run).

	2D	3D
$d/8$	4,191	263
$d/16$	68	9

Table 10. Number of LES simulations required by the MLMF algorithm for $\varepsilon^2/\varepsilon_0^2$ equal to 0.045 (with a target of 9 runs at 3D $d/16$).

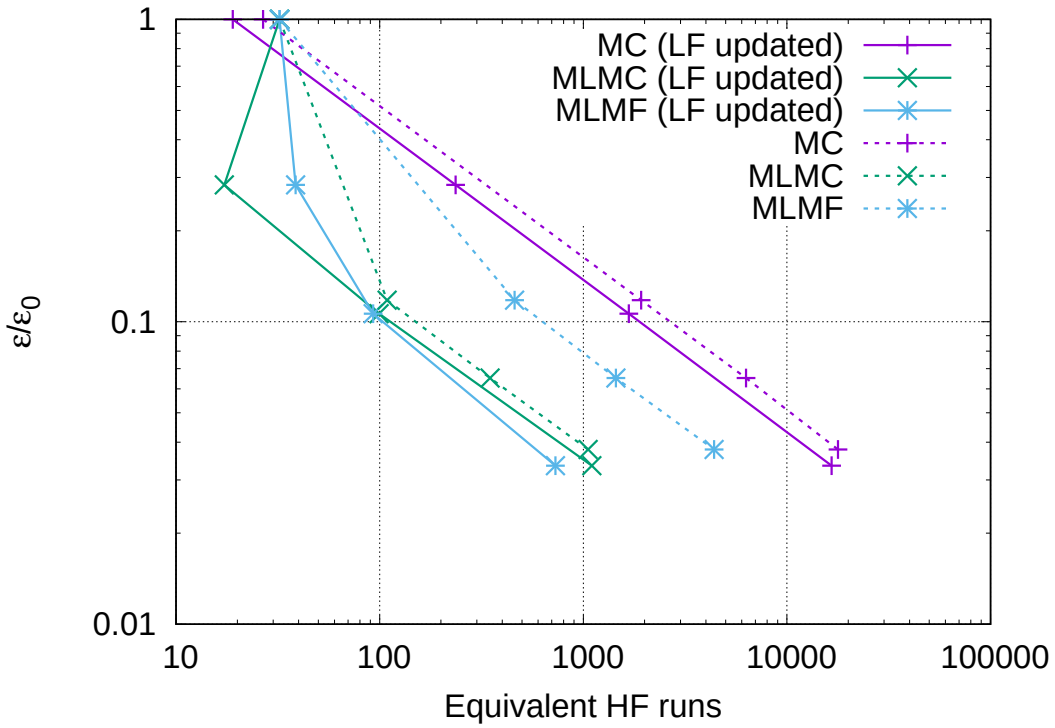

Figure 10. Nozzle problem: Standard deviation for the estimators ε normalized w.r.t. its value obtained by only pilot samples ε_0 as function of the overall computational cost in terms of equivalent number of HF fine runs.

The correlation properties on each level within the variance reduction for each separate QoI are reported in table 11. The variance reduction for the ith QoI is computed as

$$100\,(1-\Lambda_{\ell,i}) = 100\frac{r_\ell}{1+r_\ell}\rho^2_{\ell,i}, \tag{33}$$

where r_ℓ is constant across QoIs since it controls the number of additional LF simulations to evaluate.

	correlation		Variance reduction [%]	
	Coarse	Fine	Coarse	Fine
$P_{0,mean}$	0.997	0.761	93	50
$P_{0,rms,mean}$	0.875	0.593	72	30
M_{mean}	0.975	0.649	89	36
TKE_{mean}	0.824	0.454	64	17
χ_{mean}	0.450	0.714	19	44

Table 11. Correlations between 2D and 3D LES simulations and variance reduction for the five relevant QoIs in the SCRAMJET unit problem.

In figure 11 we report the performance of the MLMF estimator compared to equivalent MC and MLMC estimators in terms of aggregate variance reduction. The data are normalized in terms of the estimator accuracy obtained evaluating only the pilot samples. Moreover, the MLMC and MLMF estimators corresponding to the pilot samples are identical because during the pilot runs the low-fidelity realizations are not used for the variance but only to evaluate the correlation properties between the 2D and 3D simulations. The final normalized MSE achieved is 0.048 which corresponds to a computational cost of 49 3D LES realizations on the fine mesh for the MLMF, 151 for MLMC and 1024 for MC. The dashed lines are added in figure 11 as reference to show the expected rate of decaying of the error $\varepsilon/\varepsilon_0$.

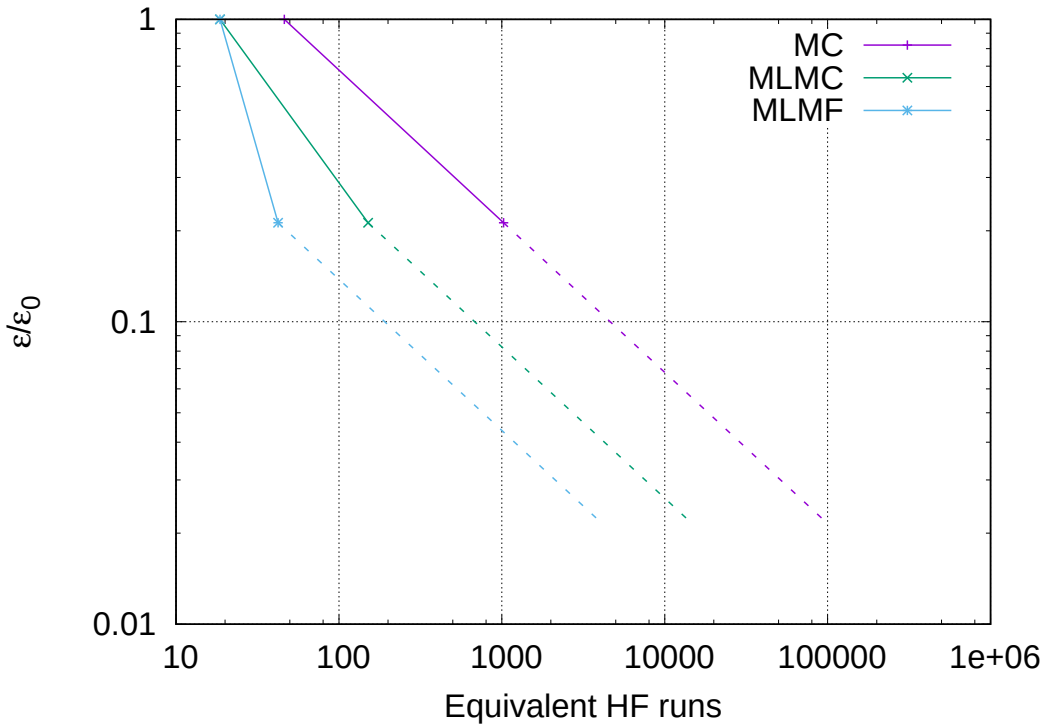

Figure 11. SCRAMJET problem: Standard deviation for the estimators ε normalized w.r.t. its value obtained by only pilot samples ε_0 as function of the overall computational cost in terms of equivalent number of HF fine runs.

X. Concluding remarks

In this work we present some recent developments in the area of multilevel estimators for forward UQ propagation analysis. In particular, the main contribution of the work is the introduction of the multifidelity control variate technique to build more efficient multilevel MC estimators. In many engineering applications the simulation of complex multiphysics problems can rely on hierarchies of model representations and numerical discretizations. The pivotal idea introduced in this manuscript is to exploit low-fidelity low computationally expensive models to reduce the statistical variance associated to estimators based on sampling methods. Moreover, numerical discretization hierarchies are also exploited to define multilevel estimators. Therefore, the method is designed to use a limited budget of HF simulations to decrease the deterministic bias of the estimator to a threshold value prescribed *a priori*; the variance properties of this estimator are improved by means of low-fidelity realizations. We focus on two applications. The first problem is an aero-thermo-structural analysis of the nozzle part of a F100-PW-220 turbofan engine which powers the Northrop Grumman X-47B unmanned combat vehicle. We use this example to derive realistic operative conditions for the engine and the nozzle. For this applications we propagated 15 uncertain parameters which comes from operative conditions, material properties and geometrical manufacturing tolerances. We demonstrated that, across a range of prescribed tolerances, the MLMF estimators are more reliable than MC and MLMC. Also we discussed the role of the correlation between the LF and HF model in order to obtain efficiently the statistics. In order to accomplish this task we also compared two different low-fidelity models with drastically different correlation behaviors. The second application is a unit problem inspired by the supersonic SCRAMJET engine HIFiRE. In this preliminary study we propagate 24 uncertain parameters related to inflow and wall boundary conditions, fuel injection, and turbulence properties. This example aims to demonstrate how the multifidelity-multilevel estimators can be employed to maximize the reliability of the statistics while matching very stringent computational cost constraints. For instance, we were able to demonstrate that with a constrained small number of high-fidelity and high-resolution 3D LES realizations, we were able to achieve a cost reduction of more than one order of magnitude with respect to a standard MC estimator. Current research directions are leaned towards the formal extension of the algorithm to multiple QoIs for which, in this manuscript, we employed an heuristic approach based on the variance aggregation across QoIs.

Acknowledgments

We gratefully acknowledge Rick Walter Fenrich, Dr. Victorien Menier and Prof. Juan Jose Alonso at Stanford University and Dr. Jason Monshke at Sandia for their invaluable support with the computations and data for the X-47B nozzle problem. We are also indebted with the Dr. Habib Najm group at Sandia Livermore (mainly Dr. Xhu Huan and Dr. Cosmin Safta) for providing us with data for the UQ analysis of the HIFiRE Scramjet. Support for this research was provided by the Defense Advanced Research Projects Agency (DARPA) program on Enabling Quantification of Uncertainty in Physical Systems (EQUiPS) led by Dr. Fariba Fahroo, Program Manager. Sandia National Laboratories is a multiprogram laboratory operated by Sandia Corporation, a Lockheed Martin Company, for the United States Department of Energy under contract DE-AC04-94-AL85000.

References

[1]J.J. Alonso, M.S. Eldred, P. Constantine, K. Duraisamy, C. Farhat, G. Iaccarino & J.D. Jakeman Scalable Environment for Quantification of Uncertainty and Optimization in Industrial Applications (SEQUOIA). *19th AIAA Non-Deterministic Approaches Conference*, Grapevine, Texas, 9-13 January, 2017.

[2]Barth, A., Schwab, Ch. & Zollinger, N. 2011 Multi-level Monte Carlo finite element method for elliptic PDEs with stochastic coefficients. *Numer. Math.* **119**(1), 123–161.

[3]Bellman, R.E. 1961 Adaptive Control Processes: A Guided Tour. Princeton University Press, 1961.

[4]Adams, B.M., Bauman, L.E., Bohnhoff, W.J., Dalbey, K.R., Ebeida, M.S., Eddy, J.P., Eldred, M.S., Geraci, G., Hooper, R.W., Hough, P.D., Hu, K.T., Jakeman, J.D., Maupin, K.A., Monschke, J.A., Rushdi, A., Swiler, L.P., Vigil, D.M., and Wildey, T.M., 2016 *Sandia Technical Report SAND2014-4633.* Updated November 2016 (Version 6.5).

[5]Cliffe, K.A., Giles, M.B., Scheichl, R. & Teckentrup, A.L. 2011 Multilevel Monte Carlo methods and applications to elliptic PDEs with random coefficients. *Comput. Vis. Sci.* **14**(1), 3–15.

[6]D.J. Dolvin Hypersonic International Flight Research and Experimentation (HIFiRE). *15th AIAA International Space Planes and Hypersonic Systems and Technologies Conference*, Dayton, Ohio, 28 April - 1 May, 2008.

[7]Doostan, A., & Owhadi, H. 2011 A non-adapted sparse approximation of PDEs with stochastic inputs. *J. Comput. Phys.* **228**(12), 4332–4345.

[8]A. Doostan, G. Geraci & G. Iaccarino 2016 A Bi-Fidelity Approach for Uncertainty Quantification of Heat Transfer in a Rectangular Ribbed Channel. *ASME Turbo Expo 2016: Turbomachinery Technical Conference and Exposition*, **2**(C), GT2016-58092.

[9]T.D. Economon, F. Palacios, S.R. Copeland, T.W. Lukaczyk & J.J. Alonso 2016 SU2: An Open-Source Suite for Multiphysics Simulation and Desig. *AIAA Journal*, **54**(3), 828–846.

[10]M.S. Eldred, G. Geraci & J.D. Jakeman Multilevel Monte-Carlo Hybrids Exploiting Multifidelity Modeling and Sparse Polynomial Chaos. *SIAM Conference on Uncertainty Quantification*, Lausanne, Switzerland, April 5-8, 2016.

[11]H. Fairbanks, A. Doostan & C. Ketelsen A Multilevel Control Variate Method Based on Low-Rank Approximation. *SIAM Conference on Uncertainty Quantification*, Lausanne, Switzerland, April 5-8, 2016.

[12]R. Fenrich 2015 F100-PW-220 Engine Model. *Private communication.*

[13]R. Fenrich 2016 F100-PW-220 Non-Ideal Nozzle Model. *Private communication.*

[14]R. Fenrich 2016 Axisymmetric Nozzle Optimization Formulations. *Private communication.*

[15]G. Geraci, M.S. Eldred & G. Iaccarino 2015 A multifidelity control variate approach for the multilevel Monte Carlo technique. *Center for Turbulence Research, Annual Research Briefs 2015*, pp. 169–181.

[16]G. Geraci, M.S. Eldred & G. Iaccarino Multilevel Monte Carlo for Convective Transport in Inhomogeneous Media. *SIAM Conference on Uncertainty Quantification*, Lausanne, Switzerland, April 5-8, 2016.

[17]G. Geraci, M.S. Eldred & G. Iaccarino Multifidelity Multilevel Monte Carlo for forward UQ. *J. Comput. Phys.* (in preparation)

[18]Giles, M.B. 2008 Multilevel Monte Carlo path simulation. *Oper. Res.* **56**, 607-617.

[19]Heinrich, S. 2001 Multilevel Monte Carlo methods *Large-Scale Scientific Computing, Third International Conference LSSC 2001, Lecture Notes in Computer Science*, Springer-Verlag, 58–67.

[20]X. Huan, C. Safta, K. Sargsyan, G. Geraci, M.S. Eldred, Z. Vane, G. Lacaze. J.C. Oefelein. & H.N. Najm Global Sensitivity Analysis and Model Error Quantification for Large Eddy Simulation of HIFiRE SCRAMJET. *19th AIAA Non-Deterministic Approaches Conference*, Grapevine, Texas, 9-13 January, 2017.

[21]K.R. Jackson, M.R. Gruber & T.F. Barhorst The HIFiRE flight 2 experiment: an overview and status update. *45th AIAA/ASME/SAE/ASEE Joint Propulsion Conference & Exhibit*, Denver, Colorado, 2-5 August, 2009.

[22]Le Maître, O. & Knio, O Spectral Methods for Uncertainty Quantification With Applications to Computational Fluid Dynamics, Springer Verlag, 2010.

[23]Liu, J.S. 2001 Monte Carlo strategies in scientific computing, Springer Verlag, 2001.

[24]Mishra, S. & Schwab, C. 2012 Sparse tensor multi-level Monte Carlo finite volume methods for hyperbolic conservation laws with random initial data. *Math. Comput.* **81**(280), 1979-2018.

[25]http://www.northropgrumman.com/MediaResources/Pages/MediaGallery.aspx?ProductId=UC-10028

[26]L.W.T. Ng & M. S. Eldred Multifidelity Uncertainty Quantification Using Non-Intrusive Polynomial Chaos and Stochastic Collocation. *53rd AIAA/ASME/ASCE/AHS/ASC Structures, Structural Dynamics and Material Conference*, 23-26 April 2012, Honolulu, Hawaii.

[27]L.W.T. Ng & K.E. Willcox 2014 Multifidelity approaches for optimization under uncertainty. *Int. J. Numer. Meth. Engng.*, **100**(10), 746–772.

[28]J.C. Oefelein 2016 Large eddy simulation of turbulent combustion processes in propulsion and power systems. *Prog. Aerosp. Sci.*, **42**(1), 2–37.

[29]Pasupathy, R., Taaffe, M., Schmeiser, B. W. & Wang, W. 2014 Control-variate estimation using estimated control means. *IIE Transactions*, **44**(5), 381–385.

[30]Poette, B., Després, B. & Lucor, D. 2009 Uncertainty quantification for systems of conservation laws. *J. Comput. Phys.* **228**, 2443-2467.

[31]Tryoen, J., Le Maître, O. & Ern, A. 2012 Adaptive anisotropic spectral stochastic methods for uncertain scalar conservation laws. *SIAM J. Sci. Comput.*, **34**(5), A2459–A2481.

[32]Z.P. Vane, G. Lacaze & J.C. Oefelein Large-Eddy Simulation of the HIFiRE Direct Connect Rig Scramjet Combustor. *19th AIAA Non-Deterministic Approaches Conference*, Grapevine, Texas, 9-13 January, 2017.